SAR Remote Sensing Flood Mapping Using A Multi-Feature Optimized Random Forest

Qinglie Yuan[a*]

[a.]School of Civil and Architecture Engineering, Panzhihua University, Panzhihua 617000, China-[*]yuanqinglie@pzhu.edu.cn

Keywords: SAR, Flood Mapping, Random Forest, Remote Sensing.

Abstract

Flood disasters, with high suddenness, wide impact and severe consequences, severely threaten ecological security, human lives, property and socioeconomic development. Optical remote sensing, though advantageous in spatial coverage and revisit frequency for flood monitoring, is heavily constrained by rainy and harsh weather accompanying floods, while Synthetic Aperture Radar (SAR) enables all-weather earth observation and thus becomes a superior alternative. Conventional SAR-based flood extraction methods such as, thresholding, object-based and standard random forest models, however, face critical limitations of high false positive rates, inaccurate land cover discrimination and poor generalization ability. To address these issues, this study proposed a robust flood mapping approach based on Sentinel-1 SAR data, taking China's Dongting Lake basin as the study area. First, Sentinel-1 data were preprocessed to extract polarization features optimal for water body identification and mapping precision. A Multiple Feature-Optimized Random Forest (MFORF) algorithm with a multi-level feature extraction framework was then developed to enhance the accuracy and reliability of flood-prone area delineation. Additionally, SAR-derived flood extents were fused with Sentinel-2-based land cover classification maps to accurately detect inundation dynamics. Quantitative and visual validations confirm that the MFORF method improves the Kappa coefficient of water extraction accuracy by an average of 3% compared with traditional SAR flood mapping techniques. This approach establishes a robust and efficient framework for rapid and accurate flood monitoring, and provides critical technical support for flood disaster response and mitigation practices.

1. Introduction

Natural disasters have long been a critical concern for human society, among which flood disasters pose severe threats to natural ecosystems, social order, and national economic development due to their high suddenness, extensive influence scope, and devastating impacts (Amitrano et al., 2024b; Lehmkuhl et al., 2022; Amitrano et al., 2021a; Tian et al., 2026). While flood disasters cannot be completely eradicated, advanced monitoring systems enable effective early warning and prevention, thereby minimizing potential losses. Among various monitoring technologies, Synthetic Aperture Radar (SAR) has gained widespread attention for its all-weather and all-time observation capabilities, which compensate for the inherent limitations of optical remote sensing. Unlike traditional real-aperture radar, SAR can acquire high-resolution imagery under diverse frequency and polarization conditions and penetrate dust and clouds with strong capacity. In contrast, electro-optical devices such as infrared sensors, despite their nighttime operation capability, suffer from poor imaging quality under adverse weather conditions, making SAR a superior alternative for flood disaster monitoring.

The integration of remote sensing and machine learning technologies has spurred innovative explorations and practices in water body and flood monitoring, driving the technological evolution toward higher precision and intelligence, accelerating multi-source data fusion, and expanding the application scope of related techniques. In agricultural flood monitoring with cross-modal data fusion, Sa´ad Ibrahim et al. (2024) proposed an integrated method of observational data and machine learning for the accurate and dynamic monitoring of flooded croplands. This method deeply fuses high-resolution multispectral satellite images capturing crop spectral features and Sentinel-1 SAR data, acquiring all-time surface information through cloud penetration, and verifies the reliability and generalization ability of the model in mapping flooded paddy field boundaries via manually labeled datasets, providing a technical paradigm for cross-modal data collaboration in rapid agricultural disaster assessment.

For spatiotemporal modeling and prediction of surface displacement, Akshar Tripath et al. (2023) focused on flood-induced surface deformation monitoring, adopting Persistent Scatterer Interferometric SAR (PSInSAR) to obtain long-term series of surface displacement data and introducing deep learning neural networks (DLNN) to construct spatiotemporal prediction models. This approach realizes high-precision inversion of surface displacement during floods and forward prediction of potential deformation trends by mining the spatiotemporal dependence of displacement data, thus providing technical support for flood disaster chain risk assessment and infrastructure protection. In exploring the application boundary of polarimetric SAR data, Adiba and Bioresita (2023) conducted an empirical study on the effectiveness of SAR polarization combinations in flood mapping, comparing the synergistic effects of VH and VV polarizations and finding that their combination failed to significantly improve the accuracy of flood boundary extraction. This conclusion reveals the limitations of single polarization features in complex surface object environments and further promotes subsequent research toward multi-polarization feature fusion.

In multi-source data-driven flood anomaly detection, Rosa Colacicco et al. (2024) developed a flood monitoring framework based on SAR data cubes and innovatively combined Gaussian process (GP) statistical modeling with geographically auxiliary data. The framework first conducts non-parametric modeling of SAR backscattering time series in normal, non-flooded areas via GP to accurately identify flood events as outliers significantly deviating from historical trends,

then fuses topographic factors derived from digital elevation models (DEM) and SAR imaging parameters to construct a multi-dimensional feature decision space. This method effectively improves the anti-noise ability of flood detection and the precision of spatial detail characterization by mining complementary information among data, serving as a typical example of multi-source heterogeneous data fusion technology in disaster monitoring.

Current international research on the integration of remote sensing and machine learning for flood monitoring exhibits two prominent characteristics: on the one hand, technological innovation presents diversity, with cutting-edge explorations including cross-modal data collaborative analysis, spatiotemporal prediction model optimization, and intelligent anomaly detection algorithm development; on the other hand, the research paradigm is undergoing profound transformation, evolving from the traditional single data processing mode to an integrated system of "data integration-model construction-scenario adaptation". These achievements not only drive the innovation of monitoring technologies but also provide universal and replicable practical solutions for global flood early warning, prevention, and scientific water resource management.

Against this backdrop, this study aims to address the existing limitations in flood monitoring through three core objectives: first, to conduct a quantitative analysis of the differences in extraction accuracy and efficiency of various methods in scenarios such as flood disaster monitoring and dynamic water resource assessment; second, to break through the limitations of single data sources and algorithms by fusing SAR polarimetric features, optical image spectral information, and topographic data, thereby enhancing the recognition ability of water body extraction for complex surface objects; third, to establish scientific and reasonable method evaluation criteria and selection guidelines, providing reusable technical solutions for flood early warning and ecological environment monitoring. Ultimately, this study seeks to achieve rapid and accurate extraction of water body information, and further provide strong technical support for disaster emergency decision-making and scientific resource management.

2. Method

This section introduces typical water body extraction methods. The most commonly used approaches for water extraction from SAR imagery include water index (WI) thresholding, object-oriented (OB) classification, and random forest (RF). Figure 1 presents the workflow for the study.

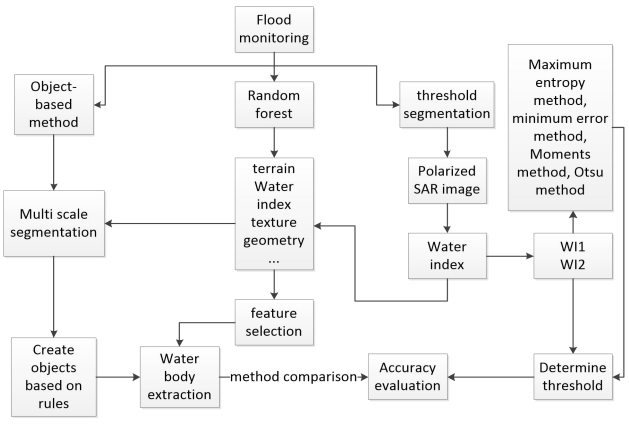

Figure 1. workflow for the SAR water extraction.

2.1 SAR Water Indices

Thresholding-based water extraction leverages the principle that water bodies exhibit low backscattering coefficients in SAR imagery. The process involves density slicing of the SAR image, determination of an optimal threshold through visual comparison, saving the sliced results as a classification file, and post-processing to eliminate false patches via human-machine interaction, ultimately yielding water body information. This method is characterized by simplicity in computation and high extraction efficiency, making it widely applied for water extraction from medium and low spatial resolution remote sensing images.

The histogram presents two distinct main peaks, indicating the presence of two land cover types, as shown in Figure 2. The target objects (water bodies marked in red area) and background areas each correspond to a peak in the histogram, with a trough region between them.

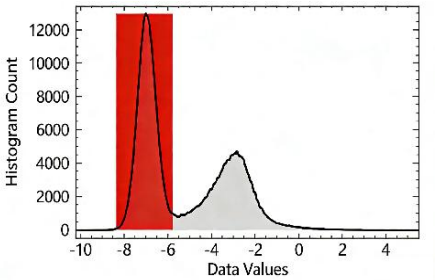

Figure 2. The histogram of SAR water indices.

The trough region contains the minimum number of pixels, and the trough value represents the boundary between the background and target areas, which can be regarded as the optimal segmentation threshold. Selecting this threshold for image slicing achieves the best extraction performance. Two water indices for SAR data are defined in Equations (1) and (2).

$$WI1 = \ln(10 \times VV \times VH) \tag{1}$$

$$WI2 = 0.1747 \times VV + 0.0082 \times VV \times VH + 0.0023 \times VV \times VV - 0.0015 \times VH \times VH + 0.190 \tag{2}$$

where VV and VH denote the backscattering coefficients of the dual-polarized bands of Sentinel-1, respectively.

2.2 Rule-Based Object-Oriented Water Extraction

Object-oriented classification technology identifies spectral features of interest by grouping adjacent pixels into objects, fully integrating spatial, textural, and spectral information of the imagery into object construction and classification. The basic processing unit of this technology is "image objects" rather than individual pixels—similar feature pixels are aggregated into meaningful object units at a specific scale following the criterion of maximizing homogeneity and minimizing heterogeneity.

The primary step of object-oriented water extraction is SAR image segmentation. To mitigate the salt-and-pepper effect to a certain extent, this study employs multi-scale segmentation on the ENVI 5.6 platform. Features including the backscattering coefficient, mean texture, and digital elevation model (DEM) of water bodies are described and converted into rules to implement rule-based object-oriented water extraction.

Image segmentation serves as the foundation and core of this method, and the selection of segmentation scale directly affects classification accuracy. This study comprehensively incorporates rules related to grayscale, texture, and shape for object-oriented classification and extraction. A multi-scale segmentation algorithm based on edge information is adopted to obtain large water body regions, followed by a merging algorithm to combine adjacent land patches as much as possible.

2.3 Random Forest Water Extraction based on Feature Selection

Random Forest (RF) is an optimized ensemble learning algorithm composed of multiple decision trees, which enhances classification performance by integrating numerous decision trees. Each decision tree is constructed based on an independent sample set generated via bootstrap sampling. Its classification error is closely associated with the classification capability of individual trees and the correlation among trees. During feature selection, node splitting is performed randomly, and the optimal feature is determined by comparing errors under different splitting strategies. The algorithm evaluates internal estimation error, classification capability, and feature correlation to adaptively select the appropriate number of features. In this study, two water indices (WI1 and WI2), DEM and eight texture features were selected, as presented in Table1.

Features selection	Feature Description	Variable Type
Dual-Polarized Water Index	WI1 and WI2	Water Index
DEM	Elevation	Terrain Feature
Mean	Grayscale mean	Texture Feature
Variance	Grayscale variance	
Homogeneity	Grayscale homogeneity	
Contrast	Grayscale contrast	
Dissimilarity	Grayscale dissimilarity	
Entropy	Grayscale entropy	
Angular Second Moment	Angular second moment	
Correlation	Grayscale correlation	

Table 1. RF-based feature selection.

Although individual decision trees have limited classification capability, the integration of a large number of random decision trees enables statistical voting on classification results of test samples to determine the final category. This ensemble strategy effectively reduces model variance and improves generalization ability, particularly demonstrating significant advantages in handling high-dimensional data and complex classification tasks. RF utilizes bootstrap sampling to draw m samples with replacement from the original training set. This sampling process is repeated n times to generate n training sets, each used to train a decision tree model. Assuming the number of sample features is d, each node splitting selects the optimal feature by calculating information gain, information gain ratio, or Gini index. Each decision tree continues splitting until all training samples in a node belong to the same category, without pruning during the splitting process. The generated n decision trees are then combined to form the RF model. For classification tasks, the final result is determined by voting among the multiple decision tree classifiers; for regression tasks, the final prediction is the average of predictions from all decision trees.

3. Study Data Description and Preprocessing

3.1 Data Description

Dongting Lake, the second-largest freshwater lake in northern Hunan (belonging to middle Yangtze River) in China, holds great strategic and economic significance, as shown in Figure 3. Its water level varies seasonally (rising in May-September with flood season, falling in October-April of next year with dry season) due to runoff from the Yangtze and four tributaries. Continuous heavy rainfall in June – July 2024 caused a sharp water level rise and dike breach risk. SAR technology enables accurate flood monitoring here. Figure 2 presents the overview map of the research area. The left image shows remote sensing images of Hunan Province, China, while the right image shows enlarged details of the Dongting Lake basin.

Figure 3. Overview map of the research area.

In this study, Sentinel-1 SAR Single Look Complex (SLC) products encompassing two polarization modes: co-polarization (VV) and cross-polarization (VH). Sentinel-2 multispectral imagery served as data sources.Mosaicking facilitates the assembly of adjacent or overlapping image swaths into a single, large-extent composite image, yielding a continuous, seamless land surface observation dataset that underpins large-scale macroscopic analyses. Ultimately, georeferenced backscatter coefficient maps corresponding to the VV and VH polarization modes were derived, as presented in Figure 4.

(a) (b)

Figure 4. SAR polarized data mosaicking results. (a) is the VH polarization and (b) is the VV polarization.

3.2 Data Preprocessing

Figure 4 illustrates the sequential preprocessing workflow for SAR data: Single Look Complex (SLC) data input is first subjected to multi-view processing, followed by filtering. The

filtered output undergoes geocoding/radiometric calibration, subsequent mosaicking, and ultimately yields the final processed results.

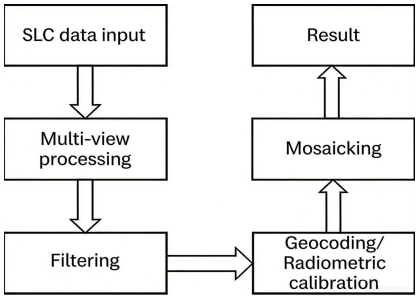

Figure 4. Flowchart of SAR preprocessing.

Given the substantial noise inherent in SAR data, a 5×5 Lee filter was applied for denoising. The resultant output, as depicted in Figure 5 (a), exhibits smoother overall grayscale distribution while effectively preserving fine details. For comparison, a 7×7 Defined Lee filter was also implemented, whose output in Figure 5 (b) displays more prominent residual noise, an artifact that may hinder accurate image interpretation and subsequent analysis. Visual comparison thus confirms that the Lee filter yields superior denoising performance for the target dataset.

(a)

(b)

Figure 5. SAR filtering results using Lee in (a) and Defined Lee in (b).

4. Experimental results

In threshold-based segmentation for water body binarization, four advanced methods including, maximum entropy, minimum error, Moments, and Otsu, were employed to address limitations of traditional thresholding, as illustrated in Figure 6.

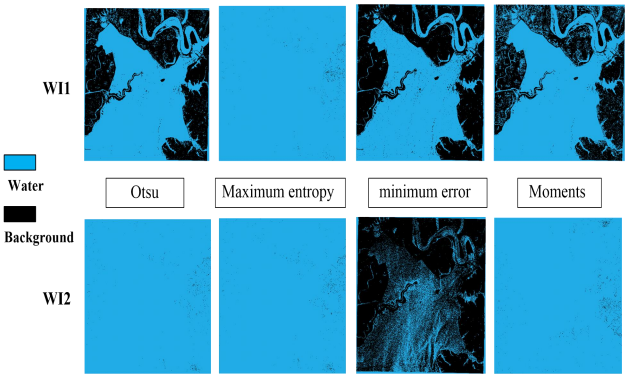

Figure 6. Threshold segmentation results for water index.

Maximum entropy method leverages grayscale distribution by selecting thresholds to maximize image information entropy rooted in information entropy theory. Minimum error method determines thresholds by minimizing misclassification probability between two land cover classes post-segmentation. Moments method identifies optimal thresholds using moment features of the image grayscale distribution. Otsu method maximizes inter-class variance to maximize the distinction between water and non-water regions.

For object-based SAR water extraction, grayscale, texture, and shape criteria were integrated with an edge-informed multi-scale segmentation algorithm to generate large water regions; adjacent patches were then merged via a merging algorithm. Parameter tuning, as depicted in Figure 7, involved: (1) fixing merging scale = 90, testing segmentation scales = 50/60/70; (2) fixing segmentation scale = 70, testing merging scales = 70/80/90. The combination with segmentation scale = 70 and merging scale = 90 was validated to balance inter-object heterogeneity and land cover patch purity, yielding superior segmentation performance.

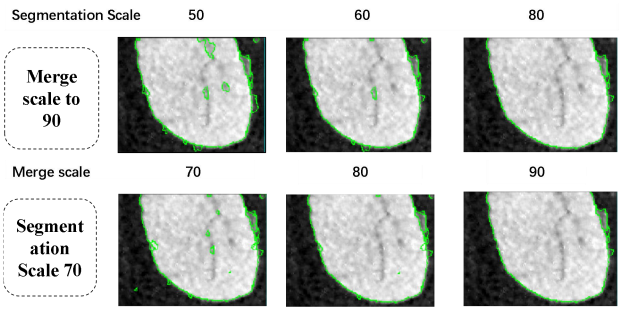

Figure 7. Object-based SAR water multi scale segmentation.

The texture features of SAR images include mean, variance, homogeneity, contrast, difference, entropy, angle matrix, and correlation, as shown in Figure 8.

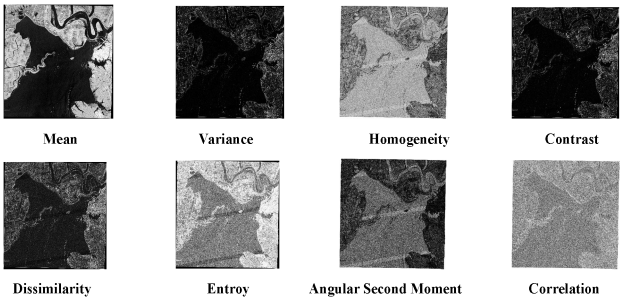

Figure 8. The texture features of SAR images.

Table 2 presents the confusion matrix and accuracy assessment results of the water body classification derived from the water index thresholding method. Quantitative analysis indicates that WI method achieved an overall accuracy (OA) of 92.47% with a Kappa coefficient of 84.80%.

Methods	OA(%)	Kappa (%)
WI	92.47	84.80
OB	95.15	68.83
RF	96.14	92.27

Table 2. Accuracy comparison using different methods

Visual comparison in Figure 9 between the extracted water maps and manually digitized reference data reveals prominent advantages in the integrity of continuous large-area water bodies, featuring naturally connected boundaries and minimal large-scale omission errors. This coefficient value demonstrates a high degree of consistency between the classification results and actual land cover, making the method suitable for extracting open water bodies with distinct spectral characteristics and relatively regular spatial distribution.

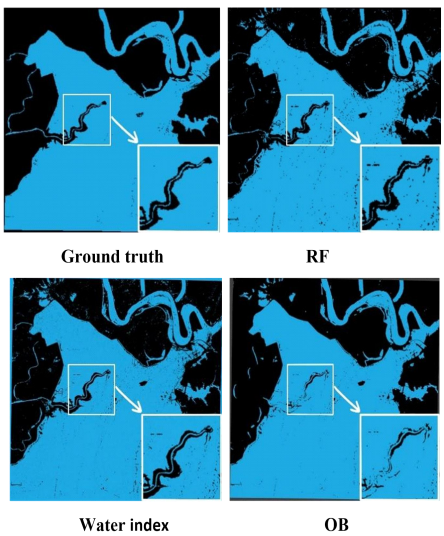

Figure 9. Visualized SAR water extraction using different methods

Although the object-based method yields a relatively high OA of 95.15%, its Kappa coefficient is merely 68.83%, indicating poor overall agreement with the ground truth. A detailed accuracy breakdown shows that the user's accuracy for non-water bodies is extremely low at 55.36%, reflecting significant misclassification errors in non-water identification.

As illustrated details in Figure 9, extensive misjudgment of non-water features as water bodies severely degrades the consistency between classification results and real-world conditions. This limitation is primarily attributed to inadequate classification rules that rely solely on partial features, as well as the empiricism inherent in rule set construction, which collectively compromises the method robustness and leads to a low Kappa coefficient.

In contrast, the random forest method with feature selection achieves the optimal consistency with actual land cover by integrating multiple decision trees to perform nonlinear fitting of multi-dimensional features, including water indices and texture attributes. This approach effectively mitigates mixed pixel interference and misclassification caused by spectral confusion between similar land cover types. Comprehensive quantitative and visual analyses confirm that among the three methods, the random forest method with feature selection outperforms the others, achieving the highest accuracy with a Kappa coefficient of 92.27% and an OA of 96.14%, validating its superiority in complex remote sensing water body extraction tasks.

In contrast, the random forest method with feature selection outperforms the other two in both accuracy and robustness. It attains the highest OA (96.14%) and Kappa (92.27%), effectively suppressing mixed pixel interference and spectral confusion via multi-dimensional feature nonlinear fitting, ensuring high consistency with actual land cover, and is more adaptable to complex SAR water extraction scenarios.

Three methods for SAR water extraction exhibit distinct differences in accuracy and performance. The thresholding method, though simple and efficient, suffers from poor anti-interference ability, easily affected by SAR noise and mixed pixels, leading to moderate OA and low consistency with ground truth. The object-based method achieves a relatively high OA but fails in stability Kappa coefficient and non-water user accuracy (55.36%) are extremely low due to empirical rule sets and incomplete feature utilization, resulting in severe non-water-to-water misclassification.

5. Conclusion

This study proposed a feature-optimized random forest (RF) method for flood extraction in Dongting Lake Basin using Sentinel-1 SAR data. Comparative experiments show this method outperforms thresholding and object-based approaches, achieving 96.14% overall accuracy and 92.27% Kappa coefficient. It effectively mitigates noise interference and spectral confusion, addressing limitations of traditional methods. This robust framework enables rapid, accurate flood mapping, providing critical technical support for flood disaster response, ecological monitoring, and water resource management in complex basins.

References

Adiba, A., Bioresita, F., 2023: Sentinel-1 SAR polarization combinations for flood inundation spatial distribution mapping (case study: South Kalimantan). *IOP Conf. Ser.: Earth Environ. Sci.*, 1127(1): 012009.

Amitrano, D., Di Martino, G., Guida, R., Iervolino, P., Iodice, A., Papa, M., Riccio, D., Ruello, G., 2021a: Earth environmental monitoring using multi-temporal synthetic aperture radar: a critical review of selected applications.*Remote Sens.*, 13: 604.

Amitrano, D., Di Martino, G., Di Simone, A., Imperatore, P., 2024b: Flood detection with SAR: a review of techniques and datasets. *Remote Sens.*, 16(4): 656.

Akshar, T., Md, M., Rafiq, A.R., et al., 2023: Chamoli flash floods of 7th February 2021 and recent deformation: a PSInSAR and deep learning neural network (DLNN) based perspective. *Nat. Hazards Res.*, 3(2): 146-154.

Colacicco, R., Refice, A., Nutricato, R., Bovenga, F., Caporusso, G., D'Addabbo, A., et al., 2024: High-resolution flood monitoring based on advanced statistical modeling of Sentinel-1 multi-temporal stacks. *Remote Sens.*, 16(2): 294.

Ibrahim, S.A., Balzter, H., 2024: Evaluating flood damage to paddy rice fields using PlanetScope and Sentinel-1 data in north-western Nigeria: towards potential climate adaptation strategies. *Remote Sens.*, 16(19): 3657.

Lehmkuhl, F., Schüttrumpf, H., Schwarzbauer, J., Brüll, C., Dietze, M., Letmathe, C.V., Hollert, H., 2022: Assessment of the 2021 summer flood in Central Europe. *Environ. Sci. Eur.*, 34: 107.

Tian, D., Wang, L., Liu, H., Cohen, S., Shu, S., 2026: DeepSAR Flood Mapper: global flood mapping on Google Earth Engine cloud platform using MLP deep learning model with Sentinel-1 SAR imagery and HAND topographic data. *GISci. Remote Sens.*, 63(1): 2612306.